Biophysical Journal
Article

Biophysical Society

Nanosecond-Timescale Dynamics and Conformational Heterogeneity in Human GCK Regulation and Disease

Shawn M. Sternisha,[1] A. Carl Whittington,[1,2] Juliana A. Martinez Fiesco,[1] Carol Porter,[1] Malcolm M. McCray,[1] Timothy Logan,[1,3] Cristina Olivieri,[4] Gianluigi Veglia,[4,5] Peter J. Steinbach,[6,*] and Brian G. Miller[1,*]

[1]Department of Chemistry and Biochemistry, [2]Department of Biological Science, and [3]Institute of Molecular Biophysics, Florida State University, Tallahassee, Florida; [4]Department of Biochemistry, Molecular Biology, and Biophysics and [5]Department of Chemistry, University of Minnesota, Minneapolis, Minnesota; and [6]Center for Molecular Modeling, Center for Information Technology, National Institutes of Health, Bethesda, Maryland

ABSTRACT Human glucokinase (GCK) is the prototypic example of an emerging class of proteins with allosteric-like behavior that originates from intrinsic polypeptide dynamics. High-resolution NMR investigations of GCK have elucidated millisecond-timescale dynamics underlying allostery. In contrast, faster motions have remained underexplored, hindering the development of a comprehensive model of cooperativity. Here, we map nanosecond-timescale dynamics and structural heterogeneity in GCK using a combination of unnatural amino acid incorporation, time-resolved fluorescence, and ^{19}F nuclear magnetic resonance spectroscopy. We find that a probe inserted within the enzyme's intrinsically disordered loop samples multiple conformations in the unliganded state. Glucose binding and disease-associated mutations that suppress cooperativity alter the number and/or relative population of these states. Together, the nanosecond kinetics characterized here and the millisecond motions known to be essential for cooperativity provide a dynamical framework with which we address the origins of cooperativity and the mechanism of activated, hyperinsulinemia-associated, noncooperative variants.

SIGNIFICANCE Allostery is a widely appreciated and ostensibly well-understood mechanism for regulating biological function. There is a growing realization that changes in protein dynamics alone can generate allostery. Human glucokinase is the prototypic example of an emerging class of proteins with allosteric-like behavior that originates from intrinsic polypeptide dynamics. The work reported here represents an important advance in understanding dynamically driven allostery in glucokinase. Using a unique combination of biophysical methods, we observe nanosecond dynamics and conformational heterogeneity associated with allostery. We find that glucose binding and disease-associated mutations that suppress cooperativity alter both the number and relative population of these states. Our results reveal important insights into the dynamical origins of cooperativity in this important glucose sensor.

INTRODUCTION

Traditional models of protein allosteric regulation have largely focused on describing the spatial transmission of ligand binding events through a polypeptide's structure (1,2). Although such models have been successful in describing cooperativity in many systems, biochemists now recognize that allostery does not require structural transitions but can also originate exclusively from altered protein dynamics (3–7). Indeed, proteins exist in a large, hierarchical ensemble of states with dynamic fluctuations and varying degrees of intrinsic disorder (8–19), and physiologically relevant allosteric regulation can involve temporal transmission of information through these states (20,21). Consequently, a comprehensive understanding of a protein's allosteric landscape requires not only a structural description of discrete conformations but also an account of the amplitude, directionality, and timescale of the dynamic motions that promote interconversion among them.

A prototypic example of nontraditional allostery, in which information is transmitted both spatially and temporally, is provided by human glucokinase (GCK) (20,22), a key regulator of glucose homeostasis in the human body

Submitted October 11, 2019, and accepted for publication December 19, 2019.

*Correspondence: bgmiller@fsu.edu or peter.steinbach@nih.gov

Editor: David Eliezer.

https://doi.org/10.1016/j.bpj.2019.12.036

(23,24). GCK displays a non-Michaelis-Menten, sigmoidal kinetic response to varying glucose concentrations—the phenomenological hallmark of cooperativity—that is essential for its role as a glucose sensor (25). In contrast to classical cooperative enzymes, such as aspartate transcarbamoylase (26), GCK functions exclusively as a monomer and possesses a single substrate binding site (Fig. 1; (25,27)). Early models, including both the mnemonic and the ligand-induced slow transition (LIST) proposals (22), posited that kinetic cooperativity can arise in monomeric enzymes from slow, "hysteretic" conformational transitions occurring on the same timescale as catalytic turnover (k_{cat}) (28,29). Since those propositions, a growing body of experimental evidence from a range of biochemical and biophysical techniques, has enabled testing and refinement of the hysteretic concept, allowing progress toward a quantitative and predictive model of the motions that underlie GCK cooperativity (30,31). For example, a global analysis of glucose binding curves suggested a minimal kinetic model involving at least two unliganded GCK conformations and four discrete enzyme-substrate binary complexes (32). Consistent with the requirements of the LIST model (33),

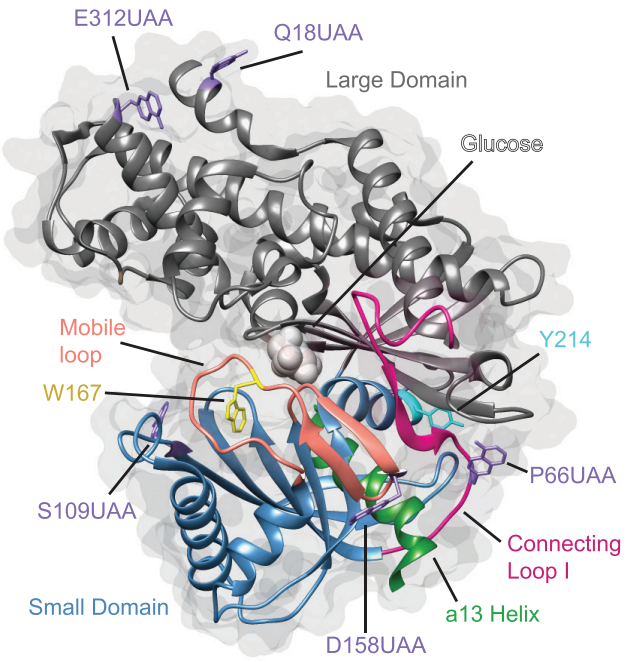

FIGURE 1 Structure of glucose-bound GCK displaying probe locations and important structural features. The large domain is gray, the small domain is blue, the bound glucose molecule is light gray, the α13 helix is green, the 151–180 mobile loop is salmon, connecting loop I is magenta, the lone Trp residue in sTrp-GCK is gold, Y214 is cyan, and the unnatural amino acid (UAA) substitution locations are purple. The SwissSideChain Chimera plugin was used to replace UAA-substituted residues with 3-(8-hydroxyquinolin-3-yl)-l-alanine as this was the most structurally similar UAA to L-(7-hydroxycoumarin-4-yl) ethylglycine (HCEG) that could be found in the database. Image was created with Protein Data Bank, PDB: 1V4S (27). To see this figure in color, go online.

the ability of these discrete conformations to interconvert during catalysis engenders GCK's cooperative response.

X-ray crystallographic studies of GCK provide insight into the conformational changes associated with the allosteric-like behavior of the enzyme. The crystal structure of GCK determined in the absence of glucose demonstrates that the enzyme adopts a super-open structure in which the large and small domains are oriented at an angle of ~100°, and the C-terminal α13 helix is solvent exposed (27). In this super-open structure, an active-site mobile loop comprised of residues 151–180 lacks electron density, suggesting that it is disordered. Upon glucose binding, GCK adopts a closed conformation characterized by an interdomain angle of 40° and a sequestered α13 helix (Fig. 1). In addition, the mobile loop is extensively stabilized by side-chain and backbone interactions with many small and large domain residues as well as water molecules (Fig. S1). The closed conformation has been observed in more than 20 GCK crystal structures to date and is largely unchanged by the presence of a nonhydrolyzable ATP analog or a small-molecule allosteric activator (34). A third conformation of GCK has also been observed when the protein was crystallized in the presence of glucose and ammonium iodide (35). This structure was termed the open structure because the angle between the large and small domains is between that of the super-open and closed states. Small-angle x-ray scattering experiments verified the existence of multiple GCK conformations in solution and support the physiological relevance of the crystallographically observed super-open and open states (35).

High-resolution NMR studies of GCK in the unliganded and glucose-bound states provide insight into the dynamic origins of cooperativity. Two-dimensional (2D) ^{1}H-^{13}C heteronuclear multiple quantum coherence (HMQC) investigations of ^{13}C-Ile methyl group labeled GCK confirm that the 151–180 loop is disordered in the unliganded state (30). Notably, crosspeaks from five additional Ile residues within the small domain were invisible on the NMR timescale, demonstrating that this region experiences millisecond conformational dynamics. Extensive deuteration afforded detection of weak crosspeaks from these small domain residues, and global fitting of a two-state model to kinetic Carr-Purcell-Meiboom-Gill NMR experiments suggests that the unliganded enzyme interconverts between a ground state and an excited state, the rate constant of which occurs on the same timescale as k_{cat} (36). Transient-state glucose binding studies also support a minimal kinetic model that involves at least two unliganded enzyme conformations that are populated to an appreciable extent (32).

Despite the characterization of stable GCK conformations via both crystallography and NMR, it is clear that the dynamic conformational transitions that produce cooperativity involve yet-to-be described substates within the unliganded ensemble. Crystallographic efforts have failed to yield more than one observable unliganded state. Similarly, the small number of

^{13}C-Ile reporters, combined with the lack of small domain crosspeaks in the NMR spectrum of unliganded GCK, limits the structural details available for describing the enzyme's conformational landscape. Identifying the ensemble of structures whose dynamic interconversion is responsible for cooperativity is essential for developing a mechanistic, predictive model for this unique form of regulation. Probing conformational dynamics is complicated by the fact that conformational ensembles, by definition, have tunable sensitivity (16), meaning that one perturbation can elicit a multitude of responses depending on the occupancies of the states that comprise the ensemble. Furthermore, the large range of timescales under which the conformational ensembles fluctuate requires a diverse suite of sensitive, complementary biophysical tools to capture motions.

Here, we map the nanosecond-timescale dynamics of GCK and the associated conformational ensemble using an array of biophysical probes. We leverage the nonsense suppression method to site-specifically incorporate a highly fluorescent, coumarin-based unnatural amino acid (fUAA) (37) into several positions in the GCK scaffold that were previously unamenable to interrogation via NMR and intrinsic protein fluorescence. We also use a single tryptophan variant of human GCK (sTrp-GCK) to investigate the structure and dynamics of the active-site mobile loop using a combination of fluorescence lifetime measurements and ^{19}F NMR. Together with past studies, our data reveal GCK conformational heterogeneity and dynamics spanning the millisecond to nanosecond timescales. The resulting picture of GCK functional dynamics provides a more comprehensive description of the events that give rise to cooperativity. Our findings also provide important insights into how the enzyme is activated by mutations that eliminate cooperativity and cause persistent hyperinsulinemic hypoglycemia of infancy (PHHI).

MATERIALS AND METHODS

Protein production

Human pancreatic GCK and variants thereof were expressed as N-terminal His_6-tagged polypeptides from pET-22b(+) in BL21(DE3) *Escherichia coli* cells. Mutations were made using the QuikChange site-directed mutagenesis kit (Agilent Technologies, Santa Clara, CA). For sTrp-GCK and α-activated sTrp-GCK production, a culture was inoculated to an initial optical density (OD_{600}) of 0.01 in lysogeny broth (LB) supplemented with ampicillin (100 μg/mL). Cells were grown at 37°C and 250 rpm until the OD_{600} reached 0.7, at which point the temperature was reduced to 20°C. Once the incubator reached 20°C, isopropyl β-D-1-thiogalactopyranoside (1 mM) was added to induce gene expression, and growth was continued for 20 h, after which time cells were harvested via centrifugation for 10 min at 6000 $\times$ *g* and 4°C.

For Y214C sTrp-GCK production, an LB-agar plate was streaked from a frozen stock of BL21(DE3) cells harboring the expression vector. An isolated colony was used to inoculate LB broth supplemented with ampicillin (100 μg/mL), and cells were grown at 37°C and 250 rpm overnight. The overnight culture was used to inoculate a 1-L expression culture to an initial OD_{600} of 0.05 in LB broth supplemented with ampicillin, and cells were grown at 37°C and 250 rpm. Once the OD_{600} reached 0.5, the cells were centrifuged for 10 min at 6000 $\times$ *g* and 20°C. The pellet was resuspended in 1 L of 37°C complete M9 media containing Na_2HPO_4 (30 g/L), KH_2PO_4 (15 g/L), NaCl (2.5 g/L) (pH 8.0), ampicillin (100 μg/mL), NH_4Cl (1 g/L), thiamine (25 μg/mL), $FeSO_4$ (10 μM), $MgSO_4$ (1 mM), 0.37 mL of Metal Mix ($FeCl_3$ (16.2 mg/L), $ZnCl_2$ (1.44 mg/L), $CoCl_2$ (1.2 mg/L), Na_2MoO_4 (1.2 mg/L), $CaCl_2$ (0.6 g/L), $CuSO_4$ (190 mg/L), H_2CO_3 (5 mg/L)), and 1.3% (v/v) glycerol as the sole carbon source. Growth was continued at 37°C and 250 rpm. Once the OD_{600} reached 5–6, the temperature on the incubator was reduced to 12°C, isopropyl β-d-1-thiogalactopyranoside (0.8 mM) was added to induce gene expression, and growth was continued for 36 h. The cells were harvested via centrifugation at 6000 $\times$ *g* and 4°C for 10 min, and cell pellets were stored at −80°C. To prepare ^{19}F-labeled proteins, the M9 media protocol described above was followed, except that 60 mg of 5-fluoroindole was dissolved in 50 μL of dimethylsulfoxide and added to the 1 L culture immediately after transfer into M9 media.

fUAA-labeled GCK was produced using the nonsense suppression method (37,38). BL21(DE3) cells were transformed with both the T7-based pET-22b(+) plasmid harboring the His_6-tagged GCK with the amber codon introduced via mutagenesis at the incorporation sites and the pEVOL plasmid containing the machinery for amber codon suppression and chloramphenicol resistance. A glycerol stock of these cells was stored at −80°C, from which a LB-agar plate supplemented with ampicillin (150 μg/mL) and chloramphenicol (25 μg/mL) was streaked. A 50-mL culture of LB broth supplemented with the same antibiotics was inoculated from a single colony and incubated overnight at 37°C. The overnight culture was used to inoculate a fresh culture, cells were grown in LB broth at 37°C until the OD_{600} reached 0.8, at which point the temperature was reduced to 20°C, and L-(7-hydroxycoumarin-4-yl) ethylglycine ((HCEG)/fUAA, 1 mM; Bachem, Bubendorf, Switzerland) and arabinose (0.02% w/v) were added to induce the expression of the transfer RNA pair. After 2 h, isopropyl β-d-1-thiogalactopyranoside (1 mM) was added to induce *gck* expression, and growth was continued for 20 h. Cells were harvested by centrifugation at 6000 $\times$ *g* and 4°C for 10 min and frozen at −80°C until use. Chemicals for protein production were purchased from Thermo Fisher Scientific (Waltham, MA) and Sigma-Aldrich (St. Louis, MO).

Protein purification

Frozen cell pellets were resuspended in cold buffer A (5 mL/g of pellet) containing either potassium phosphate (50 mM, pH 7.6) or HEPES (250 mM, pH 7.6), KCl (50 mM), dithiothreitol (DTT) (10 mM), imidazole (25 mM), and glycerol (25% (v/v)), and cells were lysed using a French press. Crude cell lysates were centrifuged at 25,000 $\times$ *g* and 4°C for 30 min, and the cleared cell lysates were loaded onto a 5-mL HisTrap FF affinity column (GE Healthcare, Chicago, IL) equilibrated in cold buffer A. The column was washed with 10 column volumes of cold buffer A, and GCK was eluted with cold buffer B (buffer A supplemented with 250 mM imidazole). GCK was dialyzed at 4°C against 1 L of size exclusion chromatography buffer containing either potassium phosphate (50 mM, pH 7.6) or HEPES (50 mM, pH 7.6), KCl (50 mM), and DTT (10 mM). After dialysis, GCK was concentrated to ~300 μM using an Amicon Ultra-15 Centrifugal Filter Unit with a MWCO of 10 kDa (MilliporeSigma, Burlington, MA) and injected onto a Superdex 200 column (GE Healthcare) pre-equilibrated in size exclusion chromatography buffer. The gel filtration column was run at a flow rate of 0.2 mL/min, and fractions containing the highest A_{280} values and relative activity were pooled and retained for analysis. Chemicals for purification were purchased from Thermo Fisher Scientific and Sigma-Aldrich.

Determination of protein concentration

The concentrations of unlabeled and fUAA-labeled GCK variants were determined spectrophotometrically at 280 nm using extinction coefficients of 32,890 M^{-1} cm^{-1} and 24,122 M^{-1} cm^{-1}, respectively. For fUAA-labeled proteins, the concentration was verified using the

extinction coefficient of HCEG at 323 nm (9222 M^{-1} cm^{-1}) after protein denaturation with 6 M guanidinium hydrochloride. The consistency between the concentrations calculated based on absorbance readings at 280 and 323 nm indicated that the purified proteins were fully labeled. Incorporation was further verified by collecting excitation (spectral peak at ~330 nm) and emission (spectral peak at ~450 nm) scans of the pure proteins and via matrix-assisted laser desorption/ionization-time-of-flight mass spectrometry.

Steady-state kinetics

GCK activity was assayed spectrophotometrically at 340 nm and 25°C on a Cary 100 Spectrophotometer by coupling the production of glucose 6-phosphate to the reduction of $NADP^+$ via glucose 6-phosphate dehydrogenase (G6PDH) or by coupling the production of ADP to the oxidation of NADH via the combined action of pyruvate kinase (PK) and lactate dehydrogenase (LDH). For G6PDH assays, reaction mixtures contained HEPES (250 mM, pH 7.6), $NADP^+$ (0.5 mM), KCl (50 mM), DTT (10 mM), ATP (0.25–10 mM), glucose (0.1–200 mM), $MgCl_2$ (12 mM), and G6PDH (7.5 units). For PK-LDH assays, reaction mixtures contained HEPES (250 mM, pH 7.6), NADH (0.25 mM), KCl (50 mM), DTT (10 mM), ATP (0.25–10 mM), glucose (0.1–200 mM), $MgCl_2$ (12 mM), PK (15 units), and LDH (15 units). Assays were performed in triplicate and initiated by the addition of ATP. The slope of the linear portion of the progress curves yielded steady-state velocities. Rate data were fitted by the Michaelis-Menten equation for ATP K_m determinations and by the Hill equation for determination of k_{cat}, glucose $K_{0.5}$, and the Hill coefficient.

Fluorescence lifetime measurements

Time-correlated single photon counting (TCSPC) was used to measure fluorescence decay curves for sTrp-GCK and fUAA variants using a FluoroMax-4 fluorescence spectrometer equipped with nano-LED light sources (HORIBA Scientific, Kyoto, Japan). Samples of 12-μM protein, with or without saturating glucose, were excited by the nano-LED (295 nm for sTrp-GCK variants; 370 nm for fUAA-labeled variants) with a repetition rate of 1 MHz. Fluorescence decay curves were collected at 335 nm for sTrp-GCK variants or 450 nm for fUAA-labeled variants, with 10-nm slit width, 95 ns of coaxial delay, and 50 ns of type allocation code range until 10,000 counts were reached. The instrument response function (IRF) was collected at 295 nm with LUDOX solution using a nano-LED 295 or at 370 nm for the nano-LED 370 with a repetition rate of 1 MHz, slit width for emission of 10 nm, 95 ns of coaxial delay, and 50 ns of time to amplitude converter (TAC) range until 10,000 counts were reached.

Fluorescence decay curves were analyzed in terms of distributions of effective lifetimes and discrete exponentials using the program MemExp (39–41), version 6.0 (available online). When described with a distribution $\boldsymbol{f}$, the TCSPC data were fit by the following expression:

$$\mathscr{F}_i = b + \int_{-\infty}^{\infty} d\log\tau\, f(\log\tau) \times \int_{t_{i-1}}^{t_i} dt \int_0^t dt'\; R(t'+\delta) e^{-(t-t')/\tau},$$

where b is the constant background, R is the instrument response function, and δ is the zero-time shift. The convolution integral was calculated using a cubic approximation of the count function for the instrument response (42). Scattered light was assumed negligible.

The $\boldsymbol{f}$ distribution was recovered for a fixed value of δ by maximizing the entropy (43)

$$S(\boldsymbol{f},\boldsymbol{F}) = -\sum_{j=1}^{M}\left[f_j \ln\left(\frac{f_j}{F_j}\right) + F_j - f_j\right]$$

while minimizing the Poisson deviance between data $\boldsymbol{D}$ and fit $\boldsymbol{\mathscr{F}}$

$$P(\boldsymbol{D},\mathscr{F}) = \frac{2}{N}\sum_{i=1}^{N}\left[D_i \ln\left(\frac{D_i}{\mathscr{F}_i}\right) + \mathscr{F}_i - D_i\right]$$

The prior model $\boldsymbol{F}$ was taken to be uniform (a constant); it is the distribution recovered in the limit of zero signal/noise (no data). Fits were assessed by the residuals, $r_i = (D_i - \mathscr{F}_i)/\sqrt{\mathscr{F}_i}$.

Brent's method of optimization and the MEM were used to find the value of δ that minimized the Poisson deviance (44). To suppress peaks that occasionally emerged in the $\boldsymbol{f}$ distribution at short lifetimes, values of δ were accepted that resulted in the mean of the fastest peak exceeding the logarithm of twice the temporal resolution of the data. In addition, if any δ values were sampled that yielded a Poisson deviance within 2% of the minimum/accepted deviance and a distribution having fewer appreciable peaks, then from this subset, the value of δ that resulted in the distribution having maximum entropy was chosen.

The preferred fits by discrete exponentials were those that resulted in at least a 1% reduction in the "reduced" Poisson deviance (given by the equation for P with 2/N replaced by $2/(N - N_{parameters})$) compared with the fit using one less exponential.

NMR experiments

Samples of ^{13}C-Ile methyl group labeled sTrp-GCK were prepared using established procedures (30), and 2D ^{1}H-^{13}C HMQC spectra were collected as previously described (31). Fluorine NMR experiments were conducted on a 600 MHz Bruker AVANCE NEO spectrometer (Bruker, Billerica, MA) equipped with a cryoprobe 5 mm TCI cryoprobe (^{1}H/^{19}F, ^{13}C, ^{15}N, and ^{2}H) with z-gradients. Free induction decay signals were recorded with a $\pi/2$ of 11 μs, a d1 of 0.7 s, 1136 complex points, 8192 scans, and spectral width of 20 parts per million (with off-set at −120 parts per million) at three different temperatures (20, 25, and 30°C). Each free induction decay was linearly predicted using an exponential multiplication function with a line broadening of 40 Hz. Spectral processing was performed using TopSpin3.5pl6 (Bruker). Samples of ^{19}F-sTrp-GCK (400 μM final concentration), with or without glucose (0.2 M), were resuspended in 3 mM $KHPO_4$ (pH 8.0), 23 mM KCl, 9 mM DTT, 5% v/v glycerol, and 10% v/v D_2O, concentrated to 300 μl and inserted in 5-mm Shigemi tubes.

RESULTS AND DISCUSSION

Human GCK contains three endogenous tryptophan residues that have proven useful in investigating the structural changes caused by ligand association and/or disease-associated mutations (29,32,45–50). Together, these past tryptophan fluorescence (TF) studies have provided strong evidence in support of global conformational heterogeneity in the unliganded state. Here, we sought to utilize time-resolved fluorescence to investigate short-timescale conformational heterogeneity and dynamics. To simplify the highly complex signals arising from the presence of multiple tryptophan residues (32), we generated a sTrp-GCK (W99C/W257F double mutant), which maintains the sigmoidal response of the native enzyme and displays

wild-type kinetic and thermodynamic characteristics (Table S1). Importantly, the 2D ^{1}H-^{13}C HMQC spectra of the enzyme containing ^{13}C-Ile methyl groups confirm that the structure of sTrp-GCK is comparable to the wild-type enzyme, both in the presence and absence of glucose (Fig. S2). The lone tryptophan residue in sTrp-GCK (W167) is located within the mobile loop near the glucose binding pocket, providing a highly sensitive, direct probe of loop conformation and dynamics. Because the loop lacks electron density in the unliganded GCK structure, and ^{13}C-Ile residues contained within the loop display overlapping chemical shift values in the NMR spectrum (36), biophysical studies of sTrp-GCK provide unique insights into the structure and dynamics of this difficult-to-interrogate disordered region.

We measured the time-dependent fluorescence of sTrp-GCK in the presence and absence of glucose using the TCSPC method and analyzed the resulting decay curves via the MemExp software (39–41). Fluorescence is exquisitely sensitive to local environment (51), and time-resolved TF decay in proteins is generally complex, requiring fitting to multiple exponential decay functions (52,53). MemExp can be used to analyze a kinetics signal in terms of a lifetime distribution and discrete exponentials without prior knowledge of the number of processes. The discrete-exponential fits are automated, and by analyzing the kinetics in terms of distributions and discrete exponentials, the range of models consistent with the experiment can be readily assessed (Figs. S3 and S4). This software has facilitated the characterization of dynamics in many physical and biochemical systems, including inferring the number of discrete steps in dihydrofolate reductase folding (39), establishing a link between DNA conformational heterogeneity and nucleic-acid mismatch recognition (54) and revealing multiple DNA conformations bound to integration host factor (44).

Representative TF decay curves for sTrp-GCK are shown in Fig. 2. It is reasonable to interpret the number of peaks in the probability distribution profile as the number of discrete conformations sampled by the fluorophore (55,56) and to assume that the peak areas reflect their relative populations. The TF decay profile of unliganded sTrp-GCK was best fit by a four-exponential decay plus baseline (Fig. 2, *top*). These states constitute the broad, nanosecond-timescale conformational ensemble sampled by the mobile loop of unliganded GCK. We postulate that the most populated species, which displays the shortest lifetime value, corresponds to the loop conformation sampled in the super-open state observed in the crystal structure of the unliganded enzyme. We posit that the other three species represent additional, appreciably populated unliganded loop conformations. The extent to which these states reflect configurations of the loop sampled by other global enzyme conformations, such as the crystallographic open and closed states, is unknown. Nonetheless, this result provides a quantitative

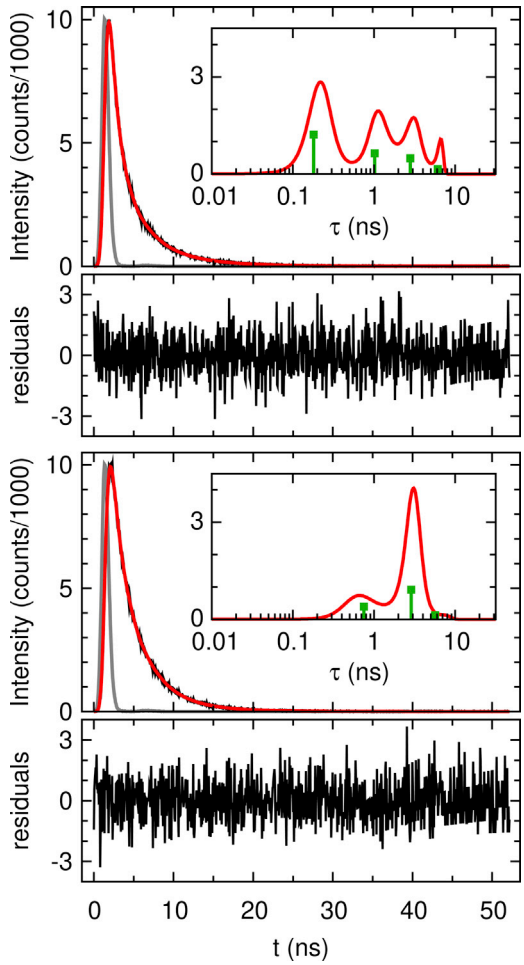

FIGURE 2 Representative fluorescence decay curves for sTrp-GCK in the absence (*top*) and presence (*bottom*) of 0.2 M glucose. The data and residuals are shown in black, the instrument response function is in gray, and the fit by lifetime distribution is in red. Insets: lifetime distribution (*red*) and discrete exponentials (*green*) recovered with MemExp. The Poisson deviances are 0.97 for both distributed and discrete (*top*) and 1.00 for both distributed and discrete (*bottom*). To see this figure in color, go online.

estimate of the number and relative population of loop conformations sampled by unliganded GCK.

In contrast to unliganded sTrp-GCK, the optimal fit of the decay curve for the glucose-bound sTrp enzyme involves three exponentials, with one species dominating the population distribution (Fig. 2, *bottom*). The most populated peak in the glucose-bound distribution likely corresponds to the loop configuration observed in the crystallographic closed conformation. In this glucose-bound structure, the side chain of W167 is involved in several hydrogen bonding interactions and van der Waals contacts with other loop residues and water molecules (Fig. S1). The two additional, weakly populated states are possibly attributable to the persistence of unliganded states arising from an inability to fully saturate the enzyme at the concentration of glucose used in this experiment (200 mM). Overall, a comparison of the tryptophan lifetime distributions of sTrp-GCK, in the

absence and presence of glucose, demonstrates that glucose binding reduces the number of accessible loop conformations and alters their relative population. This finding is consistent with the results of NMR studies on GCK containing ^{13}C-Ile probes at loop residues 159 and 163 (30).

The results of our time-resolved fluorescence studies suggest that the active-site mobile loop harboring W167 samples multiple discrete states in the absence of glucose on the nanosecond timescale. To determine whether these states persist into the millisecond regime, a timescale when other regions of the small domain are known to experience motions, we biosynthetically incorporated 5-fluoroindole into the side chain of W167 in sTrp-GCK and collected ^{19}F NMR spectra of the enzyme in the presence and absence of glucose. The ^{19}F spectra of sTrp-GCK show a single peak in the absence of glucose across a range of temperatures compatible with the retention of enzyme activity (Fig. 3 *A*). Changing the temperature altered the signal/noise ratio but failed to reveal additional peaks, as reported by the ^{19}F chemical shift value. It should be noted, however, that weakly populated states are often not observed in NMR experiments because of significant line broadening (57). The addition of 0.2 M glucose produced a slight reduction in line width, with no apparent change in peak intensity or chemical shift distribution (Fig. 3 *B*). Overlaying the spectra of unliganded and glucose-bound sTrp-GCK at 30°C confirms the similarity (Fig. 3 *C*). These results indicate that the conformational dynamics that dictate interconversion of the states detected in the time-resolved fluorescence studies are fast on the NMR timescale. We postulated that additional experimentation using a broader temperature range could perturb GCK dynamics to an appreciable extent and allow for detection of the multiple states detected using TF. However, we observed a significant reduction in signal intensity upon lowering the temperature to 20°C and a loss in enzyme activity at temperatures above 40°C, preventing further temperature variation. The lack of measurable, millisecond-timescale dynamics of the single ^{19}F reporter contrasts with the variable millisecond-timescale dynamics of Ile reporters in HMQC experiments and underscores the localized heterogeneity of GCK dynamics (Fig. S2).

PHHI is a human disease caused by gain-of-function genetic lesions in the *gck* locus that result in hyperactive, noncooperative GCK variants (58). The severity of the disease directly correlates with the level of GCK activation (59). Biophysical investigations of naturally occurring GCK mutants have led to the identification of two distinct mechanisms of enzyme activation, termed α-type and β-type (31,60). Past investigations have suggested that α-type activation results from substitutions that shift the conformational ensemble of the unliganded enzyme toward a single, glucose-bound-like state (30,31). In contrast, β-type activation is proposed to result from substitutions that accelerate the partially rate-limiting product-release step (61). To investigate the impact of each mode of activation on the structure and dynamics of the 151–180 loop, we performed time-resolved TF studies of sTrp-GCK harboring substitutions characteristic of each mechanistic class. For α-activation, we employed a previously described α13-helix variant (V452I, S453A, V455A, and A456V quadruple mutant) (62), and for β-activation, we used Y214C GCK, the most toxic naturally occurring PHHI variant reported to date (31,63).

Interestingly, the lifetime distribution recovered for the unliganded α-type variant (Fig. 4 *B*, *dashed*) is quite similar to that observed for unactivated, glucose-bound sTrp-GCK (Fig. 4 *A*, *red*). The most populated unliganded α-activated state displays a lifetime value that overlaps with the lifetime value observed for glucose-bound sTrp-GCK. The addition of glucose further increases the population of this state and reduces the conformational distribution accessible by the α-activated variant's mobile loop (Fig. 4 *B*, *red*). These results are similar to the impact of glucose binding upon the

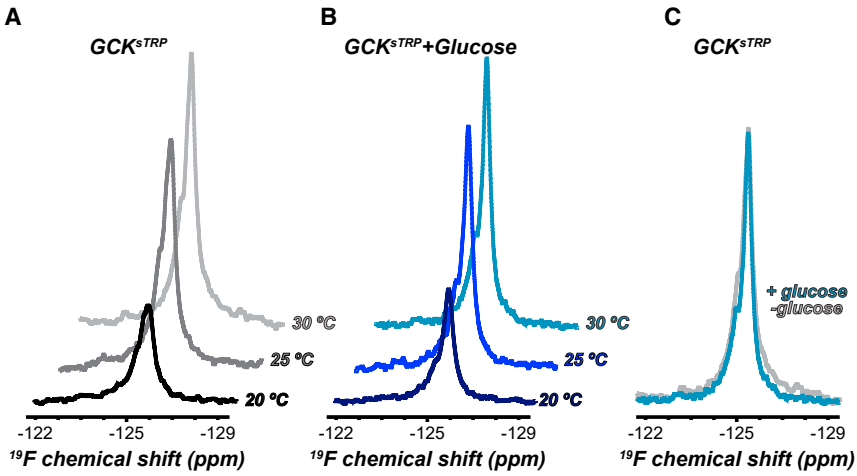

FIGURE 3 ^{19}F NMR studies of sTrp-GCK labeled with 5-fluoroindole. (*A*) Unliganded sTrp-GCK spectra at varying temperatures are shown. (*B*) Spectra of sTrp-GCK with 0.2 M glucose at varying temperatures are shown. (*C*) Overlaid spectra of unliganded and glucose-bound (0.2 M) sTrp-GCK collected at 30°C are shown. To see this figure in color, go online.

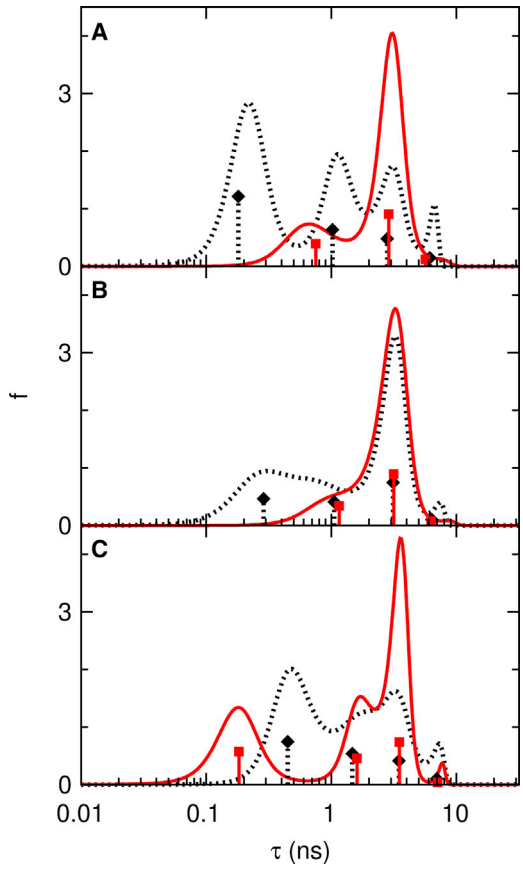

FIGURE 4 Tryptophan lifetime distributions and discrete exponentials (*vertical bars*) recovered in a MemExp analysis of experimental fluorescence decay curves obtained in the presence (*red*) and absence (*dashed*) of glucose for sTrp-GCK (*A*), α-activated sTrp-GCK (*B*), and Y214C sTrp-GCK (*C*). The Poisson deviances range from 0.97 to 1.10. To see this figure in color, go online.

lifetime distribution of unactivated sTrp-GCK. Unlike with α-activated GCK, the fluorescence lifetime distribution of the unliganded β-type variant exhibits a modest peak near 3 ns (Fig. 4 *C*, *dashed*), as observed with unliganded sTrp-GCK. Glucose addition shifts the distribution of the β-type variant toward a single state (Fig. 4 *C*, *red*), similar to the effect of glucose binding on the fluorescence lifetime distributions of other GCK variants. The lifetime value of the most populated glucose-bound state overlaps with the lifetime values of the most populated glucose-bound state of both sTrp-GCK and the α-type variant. This observation suggests that the glucose-bound loop conformation, as reported by TF lifetime distributions, is similar for all three proteins. Taken together, our data on activated GCK variants support a model in which α-activation suppresses the conformational distribution of the unliganded enzyme in favor of a loop conformation that resembles the glucose-bound species, whereas β-activation leaves the conformational ensemble of the unliganded loop largely unaltered.

Experimental methods utilizing intrinsic protein fluorescence are often limited by the fact that the quantum yield of tryptophan is low, and the frequency of tryptophan occurrence in proteins is considerably lower than most other amino acids. Therefore, naturally occurring tryptophan sites generally provide sparse information about global conformational fluctuations (64). To assess conformational dynamics at additional locations in GCK, we utilized the nonsense suppression technique to incorporate an fUAA at various positions in the enzyme (37,65,66). This technique has been extensively used to introduce fluorescent probes with high sensitivity, quantum yield, and specific excitation/emission wavelengths into proteins (37,65–68). HCEG was chosen for this purpose because of its high quantum yield, large Stokes shift, small size (264 Da), and sensitivity to pH (69).

The site-specific incorporation efficiency of unnatural amino acids (UAAs) is strongly affected by a number of factors, including the degeneracy of surrounding codons, residue packing areas, and solvent exposure (70–72). Thus, fUAA incorporation sites were selected and tested on an exhaustive basis to ensure efficient incorporation, adequate expression of the full-length product, and preservation of functional characteristics, including activity and cooperativity. We found that many of the insertion sites in the small domain significantly altered GCK's kinetic characteristics, demonstrating the importance of this domain to cooperativity and efficient catalysis. Twelve potential incorporation sites were identified based on a set of established guidelines involving solvent exposure and surrounding residues (73,74). Of the 12 variants generated, seven were not pursued because of poor incorporation, truncated products, and/or altered catalytic parameters (Table S2). The remaining acceptable variants included Q18UAA, P66UAA, S109UAA, D158UAA, and E312UAA (Fig. 1; Table S1). S109UAA, P66UAA, and D158UAA are located in the small domain, whereas Q18UAA and E312UAA are located in the large domain.

We measured the time-dependent fluorescence of individual fUAA variants in the presence and absence of glucose using the TCSPC method and analyzed the resulting decay curves via MemExp (39–41). Although nearly all of the preferred discrete-exponential fits involved multiple exponentials, the fits by a distribution indicate that a single species is predominant for all variants investigated (Figs. S5 and S6). The lifetime distributions for each fUAA probe were largely similar to one another, regardless of their location within the protein. In addition, no significant differences were observed between unliganded and glucose-bound UAA variants. These results suggest that the side chains of Q18, P66, S109, D158, and E312 do not display substantial environmental heterogeneity on the nanosecond timescale in either the unliganded or glucose-bound states. Although D158 is located within the same disordered loop as W167, the differences in lifetime distribution profiles for these positions support the existence of structural and/or dynamic heterogeneity

within the loop itself. Notably, D158 resides in a portion of the loop that folds into an antiparallel β-hairpin upon glucose binding, and the persistence of secondary structure in this region in the absence of ligand could explain its apparent reduced structural heterogeneity.

CONCLUSIONS

Previously, we have demonstrated that two key components of the GCK catalytic cycle control cooperativity. The first is a pre-existing equilibrium between unliganded GCK conformations that interconvert on the same timescale as turnover (30,36). The second is the rate of product release, which appears to be mediated by the equilibrium conformation of the intrinsically disordered 151–180 mobile loop (31,61). Past studies have provided limited structural details about the unliganded 151–180 loop, in part because this region is dynamic and disordered on the time regimes interrogated by crystallography and NMR. These results provide a unique view of the dynamic conformational landscape of the mobile loop and its relationship to GCK monomeric cooperativity. Specifically, our data demonstrate the existence of multiple, significantly populated conformations within the loop, the distribution of which is altered by activating mutations that suppress cooperativity. This observation suggests a potential interplay between the rapid dynamics of the loop and the slower dynamics of the small domain, which generate cooperativity. This interplay could include precise timing of nanosecond-timescale loop conformational sampling and millisecond-timescale hinge movements to achieve a binding-competent state, suggesting a potential physiological role for nonproductive protein motions, but this is currently speculative. The extent to which these motions, occurring on distinct timescales, are coupled to produce GCK's unique physiological function is not fully understood. Additional exploration, perhaps using advanced molecular dynamics simulations or 2D fluorescence correlation spectroscopy (75–77), is required to provide insightful connections between the motions across these disparate timescales.

In combination with past biochemical and biophysical data, the results reported herein allow us to develop a model of GCK's hierarchical functional dynamics (Fig. 5). One can envision a catalytic cycle in which the active-site mobile loop facilitates substrate binding and product release via an ability to rapidly sample multiple conformations, including those detected here. By contrast, conformational switching of the small domain between the closed, open, and super-open states is comparatively slow, as demonstrated by NMR studies. When glucose is abundant, the equilibrium among small domain conformations is shifted in favor of a more compact, catalytically competent state, and turnover is limited by the dynamics of the mobile loop. When glucose levels are low, there is sufficient time

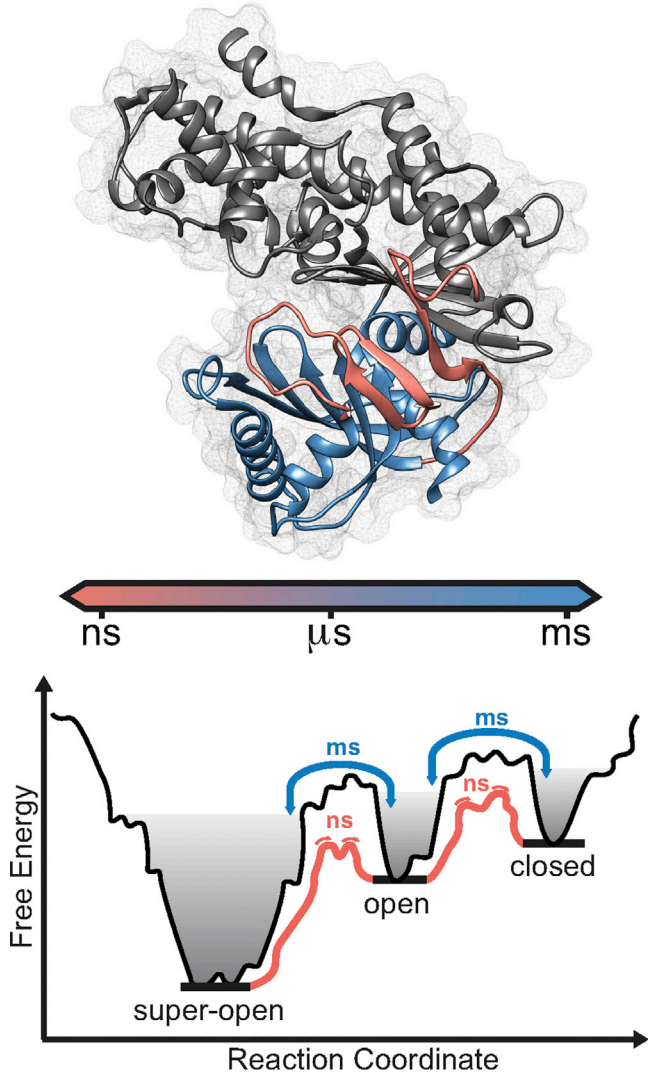

FIGURE 5 Functional dynamics of GCK. The mobile active-site loop samples multiple conformations on the nanosecond timescale (*red*), which facilitates substrate binding and product release. The small domain experiences millisecond dynamics (*blue*) that modulate interconversion between the super-open, open, and closed conformations. Cooperativity can be suppressed by β-type substitutions that accelerate product release without substantially altering the loop's nanosecond conformational heterogeneity or by α-type substitutions that alter both the nanosecond heterogeneity of the loop and the millisecond-timescale dynamics of the small domain. To see this figure in color, go online.

for relaxation of the small domain, allowing access to the inactive super-open conformation. Because the rates of interconversion and the relative population of each conformational state are strongly influenced by substrate concentration, our results support the LIST model that was first described decades ago by Neet and co-workers (33). Together, these multitimescale dynamics, which involve discrete regions of GCK's structure, provide the enzyme with exquisite sensitivity across a range of glucose concentrations, uniquely positioning it as the glucose sensor of the body.

SUPPORTING MATERIAL

Supporting Material can be found online at https://doi.org/10.1016/j.bpj.2019.12.036.

AUTHOR CONTRIBUTIONS

S.M.S., A.C.W., J.A.M.F., C.P., M.M.M., and B.G.M. designed the research. A.C.W., J.A.M.F., and B.G.M. designed the time-resolved fluorescence experiments, which were performed by A.C.W., J.A.M.F., and P.J.S. S.M.S., M.M.M., C.O., T.L., G.V., and B.G.M. designed the NMR experiments, which were performed by S.M.S., M.M.M., T.L., and C.O. A.C.W., C.P., and B.G.M. designed the unnatural amino acid experiments, which were performed by A.C.W. and C.P. S.M.S., A.C.W., P.J.S., and B.G.M. wrote the manuscript and interpreted the results. All authors reviewed the results and approved the final version of the manuscript.

ACKNOWLEDGMENTS

The authors thank Professor Peter J. Schultz for the generous gift of the pEVOL plasmid.

This work was supported by grants from the National Institutes of Health (GM115388 and GM133843) to B.G.M. and (GM100310) to G.V.. The Center for Information Technology is by the Intramural Research Program of the National Institutes of Health.

REFERENCES

1. Monod, J., J. Wyman, and J. P. Changeux. 1965. On the nature of allosteric transitions: a plausible model. *J. Mol. Biol.* 12:88–118.
2. Koshland, D. E., Jr., G. Némethy, and D. Filmer. 1966. Comparison of experimental binding data and theoretical models in proteins containing subunits. *Biochemistry.* 5:365–385.
3. Choi, J. H., A. H. Laurent, …, M. Ostermeier. 2015. Design of protein switches based on an ensemble model of allostery. *Nat. Commun.* 6:6968–6971.
4. Freiburger, L. A., O. M. Baettig, …, A. K. Mittermaier. 2011. Competing allosteric mechanisms modulate substrate binding in a dimeric enzyme. *Nat. Struct. Mol. Biol.* 18:288–294.
5. Petit, C. M., J. Zhang, …, A. L. Lee. 2009. Hidden dynamic allostery in a PDZ domain. *Proc. Natl. Acad. Sci. USA.* 106:18249–18254.
6. Tzeng, S. R., and C. G. Kalodimos. 2009. Dynamic activation of an allosteric regulatory protein. *Nature.* 462:368–372.
7. Tzeng, S. R., and C. G. Kalodimos. 2012. Protein activity regulation by conformational entropy. *Nature.* 488:236–240.
8. Austin, R. H., K. W. Beeson, …, I. C. Gunsalus. 1975. Dynamics of ligand binding to myoglobin. *Biochemistry.* 14:5355–5373.
9. Steinbach, P. J., A. Ansari, …, D. C. Lamb. 1991. Ligand binding to heme proteins: connection between dynamics and function. *Biochemistry.* 30:3988–4001.
10. Lewandowski, J. R., M. E. Halse, …, L. Emsley. 2015. Protein dynamics. Direct observation of hierarchical protein dynamics. *Science.* 348:578–581.
11. Gunasekaran, K., B. Ma, and R. Nussinov. 2004. Is allostery an intrinsic property of all dynamic proteins? *Proteins.* 57:433–443.
12. Whitford, P. C., J. N. Onuchic, and P. G. Wolynes. 2008. Energy landscape along an enzymatic reaction trajectory: hinges or cracks? *HFSP J.* 2:61–64.
13. Henzler-Wildman, K. A., M. Lei, …, D. Kern. 2007. A hierarchy of timescales in protein dynamics is linked to enzyme catalysis. *Nature.* 450:913–916.
14. Henzler-Wildman, K. A., V. Thai, …, D. Kern. 2007. Intrinsic motions along an enzymatic reaction trajectory. *Nature.* 450:838–844.
15. Kern, D., and E. R. Zuiderweg. 2003. The role of dynamics in allosteric regulation. *Curr. Opin. Struct. Biol.* 13:748–757.
16. Motlagh, H. N., J. O. Wrabl, …, V. J. Hilser. 2014. The ensemble nature of allostery. *Nature.* 508:331–339.
17. Nussinov, R., and C. J. Tsai. 2014. Free energy diagrams for protein function. *Chem. Biol.* 21:311–318.
18. Smock, R. G., and L. M. Gierasch. 2009. Sending signals dynamically. *Science.* 324:198–203.
19. Tzeng, S. R., and C. G. Kalodimos. 2011. Protein dynamics and allostery: an NMR view. *Curr. Opin. Struct. Biol.* 21:62–67.
20. Porter, C. M., and B. G. Miller. 2012. Cooperativity in monomeric enzymes with single ligand-binding sites. *Bioorg. Chem.* 43:44–50.
21. Hilser, V. J., J. A. Anderson, and H. N. Motlagh. 2015. Allostery vs. "allokairy". *Proc. Natl. Acad. Sci. USA.* 112:11430–11431.
22. Larion, M., and B. G. Miller. 2012. Homotropic allosteric regulation in monomeric mammalian glucokinase. *Arch. Biochem. Biophys.* 519:103–111.
23. Wilson, J. E. 1995. Hexokinases. *Rev. Physiol. Biochem. Pharmacol.* 126:65–198.
24. Ferre, T., E. Riu, …, A. Valera. 1996. Evidence from transgenic mice that glucokinase is rate limiting for glucose utilization in the liver. *FASEB J.* 10:1213–1218.
25. Matschinsky, F. M. 1990. Glucokinase as glucose sensor and metabolic signal generator in pancreatic β-cells and hepatocytes. *Diabetes.* 39:647–652.
26. Kantrowitz, E. R. 2012. Allostery and cooperativity in *Escherichia coli* aspartate transcarbamoylase. *Arch. Biochem. Biophys.* 519:81–90.
27. Kamata, K., M. Mitsuya, …, Y. Nagata. 2004. Structural basis for allosteric regulation of the monomeric allosteric enzyme human glucokinase. *Structure.* 12:429–438.
28. Frieden, C. 1970. Kinetic aspects of regulation of metabolic processes. The hysteretic enzyme concept. *J. Biol. Chem.* 245:5788–5799.
29. Lin, S. X., and K. E. Neet. 1990. Demonstration of a slow conformational change in liver glucokinase by fluorescence spectroscopy. *J. Biol. Chem.* 265:9670–9675.
30. Larion, M., R. K. Salinas, …, R. Brüschweiler. 2012. Order-disorder transitions govern kinetic cooperativity and allostery of monomeric human glucokinase. *PLoS Biol.* 10:e1001452.
31. Whittington, A. C., M. Larion, …, B. G. Miller. 2015. Dual allosteric activation mechanisms in monomeric human glucokinase. *Proc. Natl. Acad. Sci. USA.* 112:11553–11558.
32. Larion, M., and B. G. Miller. 2010. Global fit analysis of glucose binding curves reveals a minimal model for kinetic cooperativity in human glucokinase. *Biochemistry.* 49:8902–8911.
33. Ainslie, G. R., Jr., J. P. Shill, and K. E. Neet. 1972. Transients and cooperativity. A slow transition model for relating transients and cooperative kinetics of enzymes. *J. Biol. Chem.* 247:7088–7096.
34. Nishimura, T., T. Iino, …, J. Eiki. 2009. Identification of novel and potent 2-amino benzamide derivatives as allosteric glucokinase activators. *Bioorg. Med. Chem. Lett.* 19:1357–1360.
35. Liu, S., M. J. Ammirati, …, X. Qiu. 2012. Insights into mechanism of glucokinase activation: observation of multiple distinct protein conformations. *J. Biol. Chem.* 287:13598–13610.
36. Larion, M., A. L. Hansen, …, R. Brüschweiler. 2015. Kinetic cooperativity in human pancreatic glucokinase originates from millisecond dynamics of the small domain. *Angew. Chem. Int.Engl.* 54:8129–8132.
37. Wang, L., and P. G. Schultz. 2004. Expanding the genetic code. *Angew. Chem. Int.Engl.* 44:34–66.
38. Liu, C. C., and P. G. Schultz. 2010. Adding new chemistries to the genetic code. *Annu. Rev. Biochem.* 79:413–444.

39. Steinbach, P. J., R. Ionescu, and C. R. Matthews. 2002. Analysis of kinetics using a hybrid maximum-entropy/nonlinear-least-squares method: application to protein folding. *Biophys. J.* 82:2244–2255.

40. Steinbach, P. J. 2002. Inferring lifetime distributions from kinetics by maximizing entropy using a bootstrapped model. *J. Chem. Inf. Comput. Sci.* 42:1476–1478.

41. Steinbach, P. J. 2012. Filtering artifacts from lifetime distributions when maximizing entropy using a bootstrapped model. *Anal. Biochem.* 427:102–105.

42. Bajzer, Z., M. C. Moncrieffe, …, F. G. Prendergast. 2001. Complex homogeneous and heterogeneous fluorescence anisotropy decays: enhancing analysis accuracy. *Biophys. J.* 81:1765–1775.

43. Skilling, J. 1989. Classic maximum entropy. *In* Maximum Entropy and Bayesian Methods. J. Skilling, ed. Springer Dordrecht, pp. 45–52.

44. Connolly, M., A. Arra, …, A. Ansari. 2018. Static kinks or flexible hinges: multiple conformations of bent DNA bound to integration host factor revealed by fluorescence lifetime measurements. *J. Phys. Chem. B.* 122:11519–11534.

45. Cárdenas, M. L., E. Rabajille, …, H. Niemeyer. 1985. Cooperative interactions in hexokinase D ("glucokinase"). Kinetic and fluorescence studies. *Arch. Biol. Med. Exp. (Santiago).* 18:273–284.

46. Zelent, B., S. Odili, …, F. M. Matschinsky. 2008. Sugar binding to recombinant wild-type and mutant glucokinase monitored by kinetic measurement and tryptophan fluorescence. *Biochem. J.* 413:269–280.

47. Zelent, B., S. Odili, …, F. M. Matschinsky. 2011. Mutational analysis of allosteric activation and inhibition of glucokinase. *Biochem. J.* 440:203–215.

48. Zelent, B., C. Buettger, …, F. M. Matschinsky. 2012. Thermal stability of glucokinase (GK) as influenced by the substrate glucose, an allosteric glucokinase activator drug (GKA) and the osmolytes glycerol and urea. *Biochim. Biophys. Acta.* 1824:769–784.

49. Zelent, B., A. Raimondo, …, F. M. Matschinsky. 2014. Analysis of the co-operative interaction between the allosterically regulated proteins GK and GKRP using tryptophan fluorescence. *Biochem. J.* 459:551–564.

50. Zelent, B., C. Bialas, …, F. M. Matschinsky. 2017. Tryptophan fluorescence yields and lifetimes as a probe of conformational changes in human glucokinase. *J. Fluoresc.* 27:1621–1631.

51. Berezin, M. Y., and S. Achilefu. 2010. Fluorescence lifetime measurements and biological imaging. *Chem. Rev.* 110:2641–2684.

52. Alcala, J. R., E. Gratton, and F. G. Prendergast. 1987. Fluorescence lifetime distributions in proteins. *Biophys. J.* 51:597–604.

53. Alcala, J. R., E. Gratton, and F. G. Prendergast. 1987. Interpretation of fluorescence decays in proteins using continuous lifetime distributions. *Biophys. J.* 51:925–936.

54. Chakraborty, S., P. J. Steinbach, …, A. Ansari. 2018. Enhanced spontaneous DNA twisting/bending fluctuations unveiled by fluorescence lifetime distributions promote mismatch recognition by the Rad4 nucleotide excision repair complex. *Nucleic Acids Res.* 46:1240–1255.

55. Lu, M., and H. P. Lu. 2014. Probing protein multidimensional conformational fluctuations by single-molecule multiparameter photon stamping spectroscopy. *J. Phys. Chem. B.* 118:11943–11955.

56. DeVore, M. S., A. Braimah, …, C. K. Johnson. 2016. Single-molecule FRET states, conformational interchange, and conformational selection by dye labels in calmodulin. *J. Phys. Chem. B.* 120:4357–4364.

57. Mittermaier, A., and L. E. Kay. 2006. New tools provide new insights in NMR studies of protein dynamics. *Science.* 312:224–228.

58. Glaser, B., P. Kesavan, …, K. C. Herold. 1998. Familial hyperinsulinism caused by an activating glucokinase mutation. *N. Engl. J. Med.* 338:226–230.

59. Osbak, K. K., K. Colclough, …, A. L. Gloyn. 2009. Update on mutations in glucokinase (GCK), which cause maturity-onset diabetes of the young, permanent neonatal diabetes, and hyperinsulinemic hypoglycemia. *Hum. Mutat.* 30:1512–1526.

60. Sternisha, S. M., and B. G. Miller. 2019. Molecular and cellular regulation of human glucokinase. *Arch. Biochem. Biophys.* 663:199–213.

61. Sternisha, S. M., P. Liu, …, B. G. Miller. 2018. Mechanistic origins of enzyme activation in human glucokinase variants associated with congenital hyperinsulinism. *Biochemistry.* 57:1632–1639.

62. Larion, M., and B. G. Miller. 2009. 23-Residue C-terminal alpha-helix governs kinetic cooperativity in monomeric human glucokinase. *Biochemistry.* 48:6157–6165.

63. Cuesta-Muñoz, A. L., H. Huopio, …, M. Laakso. 2004. Severe persistent hyperinsulinemic hypoglycemia due to a de novo glucokinase mutation. *Diabetes.* 53:2164–2168.

64. Clayton, A. H., and W. H. Sawyer. 2002. Site-specific tryptophan fluorescence spectroscopy as a probe of membrane peptide structure and dynamics. *Eur. Biophys. J.* 31:9–13.

65. Wang, L., A. Brock, …, P. G. Schultz. 2001. Expanding the genetic code of *Escherichia coli*. *Science.* 292:498–500.

66. Cropp, T. A., and P. G. Schultz. 2004. An expanding genetic code. *Trends Genet.* 20:625–630.

67. Leisle, L., F. Valiyaveetil, …, C. A. Ahern. 2015. Incorporation of noncanonical amino acids. Novel Chemical Tools to Study Ion Channel Biology. Springer, pp. 119–151.

68. Xiao, H., A. Chatterjee, …, P. G. Schultz. 2013. Genetic incorporation of multiple unnatural amino acids into proteins in mammalian cells. *Angew. Chem. Int.Engl.* 52:14080–14083.

69. Wang, J., J. Xie, and P. G. Schultz. 2006. A genetically encoded fluorescent amino acid. *J. Am. Chem. Soc.* 128:8738–8739.

70. Bossi, L., and J. R. Roth. 1980. The influence of codon context on genetic code translation. *Nature.* 286:123–127.

71. Miller, J. H. 1991. Use of nonsense suppression to generate altered proteins. *Methods Enzymol.* 208:543–563.

72. Wals, K., and H. Ovaa. 2014. Unnatural amino acid incorporation in *E. coli*: current and future applications in the design of therapeutic proteins. *Front Chem.* 2:15.

73. Kleina, L. G., J. M. Masson, …, J. H. Miller. 1990. Construction of *Escherichia coli* amber suppressor tRNA genes. II. Synthesis of additional tRNA genes and improvement of suppressor efficiency. *J. Mol. Biol.* 213:705–717.

74. Normanly, J., L. G. Kleina, …, J. H. Miller. 1990. Construction of *Escherichia coli* amber suppressor tRNA genes. III. Determination of tRNA specificity. *J. Mol. Biol.* 213:719–726.

75. Kapusta, P., M. Wahl, …, J. Enderlein. 2007. Fluorescence lifetime correlation spectroscopy. *J. Fluoresc.* 17:43–48.

76. Ishii, K., and T. Tahara. 2013. Two-dimensional fluorescence lifetime correlation spectroscopy. 1. Principle. *J. Phys. Chem. B.* 117:11414–11422.

77. Otosu, T., K. Ishii, and T. Tahara. 2015. Microsecond protein dynamics observed at the single-molecule level. *Nat. Commun.* 6:7685.